JOURNAL OF EXPERIMENTAL AND THEORETICAL PHYSICS, 2024, Vol. 165, No. 3, pp. 374–389

SOLID BODIES AND LIQUIDS

PREDICTION OF LOW-TEMPERATURE SILVER SULFIDE PHASES, DERIVATIVE FROM ARGENTITE

© 2024 S.I. Sadovnikov [a], M.G. Kostenko [a], A.I. Gusev [a*], A.V. Lukoyanov [b,c]

[a] Institute of Solid State Chemistry Ural Branch of Russian Academy of Sciences, 620990, Yekaterinburg, Russia
[b] Mikheev Institute of Metal Physics, Ural Branch of the Russian Academy of Sciences, 620108, Yekaterinburg, Russia
[c] First President of Russia Boris Yeltsin Ural Federal University, 620002, Yekaterinburg, Russia
* e-mail: gusev@ihim.uran.ru

Received September 15, 2023
Revised October 19, 2023
Accepted October 20, 2023

Abstract. Such phases of silver sulfide as body-centered cubic argentite and monoclinic acanthite are widely known. Traditionally, acanthite is considered as the only low-temperature phase of silver sulfide. Low-temperature monoclinic acanthite can be considered as a result of the ordering of sulfur atoms in a non-metallic volume-centered cubic sublattice of argentite, accompanied by a redistribution of silver atoms. However, the possible existence of other low-temperature phases of silver sulfide cannot be excluded. The search for the model phases of the silver sulfide was performed using an evolutionary algorithm. The possibility of the formation of Ag_2S phases with cubic, tetragonal, orthorhombic, trigonal, monoclinic and triclinic symmetries is considered. The calculation of the cohesion energy and enthalpy of formation showed that the formation of low-symmetry phases of Ag_2S is energetically most favorable. The elastic stiffness constants c_{ij} of all predicted phases of Ag_2S are calculated and their mechanical stability is determined. The electron state densities of the predicted Ag_2S phases are calculated. Channels of disorder-order transitions associated with the formation of low-temperature unrelaxed monoclinic acanthite α-Ag_2S and cubic (space group $Pn\bar{3}m$) silver sulfide Ag_2S from disordered argentite have been found. The spatial distributions of Young's modulus and comprehensive compression of cubic (space group $Pn\bar{3}m$) silver sulfide Ag_2S are determined and a weak anisotropy of its elastic properties is established.

Keywords: *silver sulfide*; *crystal structure predictions*; *formation enthalpy*; *electronic structure*; *elastic constants*; *mechanical stability*

DOI: 10.31857/S00444510240307e1

1. INTRODUCTION

The main phases of silver sulfide Ag_2S are monoclinic (space group $P2_1/c$) acanthite α-Ag_2S and body-centered cubic (space group $Im\bar{3}m$) argentite β-Ag_2S [1]. Upon cooling of BCC-argentite β-Ag_2S below temperature 450 K, a phase transition occurs with the formation of monoclinic acanthite α-Ag_2S [2]. In cubic arginite β-$Ag_{2\pm\delta}Sc$ with $\delta \approx 0.002$ there may be both a small deficit and a small excess of silver. Large-crystalline (bulk) monoclinic acanthite α-Ag_2S is stoichiometric, whereas silver sulfide nanoparticles with a size of less than 50 nm are non-stoichiometric, have a composition $Ag_{1.93}S$ and contain vacant nodes in a metal sublattice [3].

According to [4, 5], the structure of acanthite α-Ag_2S is the result of distortion of the BCC sublattice of sulfur atoms S in the structure of argentite β-Ag_2S. The transformation of argentite – acanthite is accompanied by distortion of the BCC sublattice of atoms S to a monoclinic sublattice and displacements of sulfur and silver atoms [6]. In general, the transformation of BCC-argentite into low-temperature monoclinic acanthite can be considered as an ordering of sulfur atoms in the BCC sublattice S [7]. A variant of the argentite ordering with the

formation of a monoclinic (space group $P2_1$) phase Ag_2S was proposed in [8]. Apparently, when the temperature decreases in silver sulfide, other phases of silver sulfide Ag_2S with different structures may form in addition to acanthite. Possible model phases of silver sulfide Ag_2S can have cubic, tetragonal, orthorhombic, trigonal, monoclinic and triclinic symmetries.

The prediction of possible model phases of silver sulfide having a structure different from monoclinic acanthite is important for the production of silver sulfides and sulfide heteronostructures of the type Ag_2S/ZnS with an adjustable band gap, which will expand the potential use of both sulfides Ag_2S and heterostructures Ag_2S/ZnS. In particular, the use of silver sulfide phases, which differ in structure from monoclinic acanthite, due to the higher switching speed, will make it possible to improve Ag_2S/Ag resistive switches and non-volatile memory devices operating on the basis of heterostructures. In addition, silver sulfide phases, which differ from monoclinic acanthite, can be used for the photocatalytic oxidation of impurities in water, as well as for the photocatalytic splitting of water as a method for producing hydrogen. It is the potential possibility of the existence of low-temperature phases of silver sulfide, which are derivatives of high-temperature arginite β-Ag_2S but different from acanthite α-Ag_2S, that has aroused interest in modeling such structures. Note that Ag_2S no one has experimentally observed low-temperature phases other than acanthite, since the transformation of the crystal structure of acanthite at temperatures below 300 K is kinetically difficult, and the diffraction patterns of possible related phases of Ag_2S are difficult to distinguish.

When modeling Ag_2S phases, it was taken into account that the nearest distances between atoms Ag should be greater than twice the atomic radius of silver, equal to 0.144–0.146 nm [9], i.e. greater than 0.288–0.292 nm. In other words, Ag atoms in the model phases of silver sulfide Ag_2S can be at least 0.288–0.292 nm apart from each other. Their enthalpy of formation and cohesion energies were calculated as the energy characteristics of the model phases Ag_2S, and calculated elastic stiffness constants were used to assess the mechanical stability of the predicted phases c_{ij}.

2. MODELING METHODS

The search for possible model phases of Ag_2S was performed using the USPEX (Universal Structure Predictor: Evolutionary Xtallography) program [10]. The USPEX evolutionary algorithm used to predict and model the crystal structures of silver sulfides is described in detail in [11 — 13].

The total energy of the predicted model structures was calculated by the electron density functional (DFT) method [14] using the generalized gradient approximation (GGA) in version [15] and the projection coupled wave method (PAW) [16] implemented in the VASP code (Vienna ab initio simulation package) [17]. Stepwise relaxation to determine the equilibrium parameters of elementary cells and atomic positions was carried out using the USPEX evolutionary algorithm [10], as well as using the conjugate gradient algorithm and the quasi-Newtonian RMM-DIIS algorithm presented in the VASP software package [18].

The thermodynamic stability of the model phases of silver sulfides Ag_2S with different crystal structures was estimated by their enthalpy of formation ΔH_f at $T = 0$K and $P = 0$ by the reaction $2Ag + S = Ag_2S$ from metallic silver Ag (space group 225 - $Fm\bar{3}m$) and orthorhombic sulfur S (space group 70 — *Fddd*). The enthalpy of formation of the ΔH_f predicted phases was Ag_2S determined taking into account the real number of atoms in the elementary cells Ag, S and Ag_2S. An elementary cell of metallic silver contains four atoms Ag ($N_{Ag-cond} = 4$), an elementary cell of orthorhombic sulfur S contains 128 atoms S ($N_{S-cond} = 128$), and the predicted phase Ag_2S contains Z formula units. The number of formula units Ag_2S coincides with the number of atoms S in the predicted phase. With this in mind, the enthalpy of ΔH_f phase formation was Ag_2S determined by the formula

$$\Delta H_f = \frac{1}{Z}\left[E_{phase} - \frac{N_{Ag} E_{Ag-cond}}{N_{Ag-cond}} - \frac{N_S E_{S-cond}}{N_{S-cond}}\right], \quad (1)$$

where E_{phase} is the energy of the predicted phase of Ag_2S, $E_{Ag-cond} = -10.86$ eV is the energy of condensed metallic silver Agwith cubic (spatial group $Fm\bar{3}m$) structure, $E_{S-cond} = -528.17$ eV is the energy of condensed sulfur S with orthorhombic (space group *Fddd*) structure, $N_{Ag}$and N_S— the

number of atoms Ag and S in the unit cell of the predicted phase of Ag_2S; Z — the number of formula units in the predicted phase Ag_2S. Dividing by Z normalizes values ΔH_f by one formula unit Ag_2S (i.e., by one atom S). Energies E_{phase}, $E_{Ag-cond}$ and E_{S-cond} were pre-calculated by the electron density functional method in the VASP software package.

The electronic structure and total phase energy Ag_2S were studied within the framework of density functional theory [14] using the generalized gradient approximation [15] and the projection coupled wave method [17] implemented in the VASP code [16, 18]. The density diagrams of electronic states (DOS) were calculated using the tetrahedron method with Blöchl corrections [19]. The curves of the zone structure were constructed along the trajectories of k-points using the SeeK-path tool proposed in [20].

The elastic stiffness constants c_{ij} were calculated by the finite difference method implemented in the VASP software package [16, 17, 18]. The mechanical stability of the model structures was determined using the necessary and sufficient criteria given in [21].

3. RESULTS AND DISCUSSION

According to the USPEX evolutionary algorithm, along with monoclinic acanthite, α-Ag_2S cubic (space groups $Pn\bar{3}m$ and $Fd\bar{3}m$), tetragonal (space groups $P\bar{4}c2$ and $P4/mmm$) and trigonal (space groups $R\bar{3}$ and $R\bar{3}m$) phases can presumably be formed as alternative low-temperature phases of Ag_2S.

The energy characteristics of these model phases Ag_2S, predicted using the USPEX code, are shown in Table 1.

The elementary cells of the model cubic, tetragonal and trigonal phases of Ag_2S, which presumably can be formed as alternative low-temperature phases along with monoclinic acanthite α-Ag_2S, are shown in Fig. 1.

The translation vectors and atomic coordinates in the elementary cells of these model phases of Ag_2S are shown in Table 2.

All these model crystal structures, as well as the predicted orthorhombic, monoclinic and triclinic

Table 1. The calculated enthalpy of formation ΔH_f and the complete decrease in symmetry of the N_{tot} predicted phases of silver sulfide. E_{phase} — the energy of the predicted structure Ag_2S, calculated by the DFT method in the VASP code

Symmetry and space group	Number of atoms		Z	E_{phase}, eV	ΔH_f, eV/(Ag_2S units)	N_{tot}
	N_{Ag}	N_S				
Cubic (224–$Pn\bar{3}m$)	4	2	2	–19.498	–0.191	1.5
Cubic (227–$Fd\bar{3}m$)	32	16	16	–95.749	3.573	8
Tetragonal (116–$P\bar{4}c2$)	8	4	4	–36.655	0.394	12
Tetragonal (123–$P4\ /\ mmm$)	2	1	1	–8.2445	1.313	1.5
Trigonal (148–$R\bar{3}$)	2	1	1	–9.516	0.042	4
Trigonal (166–$R\bar{3}m$)	4	2	2	–19.033	0.041	4
Orthorhombic (64– $Cmce$)	16	8	8	–78.216	–0.219	30
Orthorhombic (63– $Cmcm$)	8	4	4	–39.027	–0.199	12
Monoclinic (14–$P2_1/c$) unrelaxed acanthite	8	4	4	–38.361	–0.033	24
Monoclinic (14–$P2_1/c$) relaxed acanthite	8	4	4	–39.028	–0.199	30
Monoclinic (14–$P2_1/c$)	8	4	4	–39.107	–0.219	36
Triclinic (1–$P1$)	8	4	4	–39.125	–0.223	96

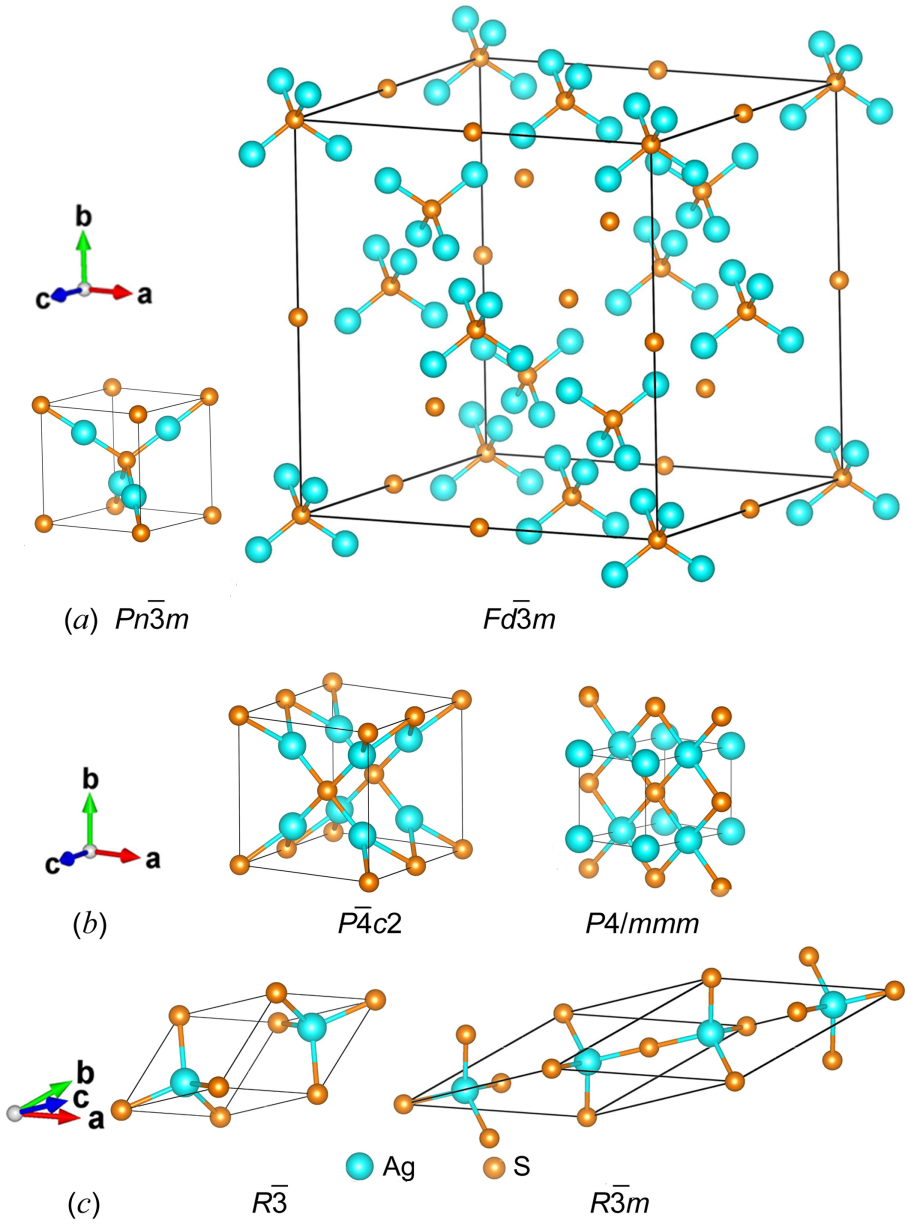

Fig. 1. Unit cells of possible ordered structures of Ag_2S derived from argentite: *a* — model cubic phases of Ag_2S with space groups 224—$Pn\bar{3}m$ and 227—$Fd\bar{3}m$, *b* — model tetragonal phases of Ag_2S with space groups 116— $P\bar{4}c2$ and 123—$P4/mmm$, *c* — model trigonal phases of Ag_2S with space groups 148 — $R\bar{3}$ and 166 —$R\bar{3}m$

structures described below, Ag_2S were visualized using the VESTA program [22].

The enthalpy of formation of ΔH_f model cubic phases Ag_2S with space groups $Pn\bar{3}m$ and $Fd\bar{3}m$, shown in Fig. 1*a*, are equal to $-0.191 + 3.573$ eV/form. units (see Table 1). It is clear that the formation of a model cubic (space group $Fm\bar{3}m$) phase of Ag_2S is thermodynamically impossible, whereas a model cubic (space group $Pn\bar{3}m$) structure of Ag_2S is quite advantageous in terms of the enthalpy of formation. Model tetragonal structures of Ag_2S with space groups $P\bar{4}c2$ and $P4/mmm$ calculated in the USPEX code are shown in Fig. 1*b*. The enthalpy of formation of ΔH_f of these structures is equal to $+0.394 + 1.313$ eV/form. units (see Table 1). Judging by the positive values of the enthalpy of formation of ΔH_f, the formation of such tetragonal structures of silver sulfide is energetically impossible. The calculated enthalpy of formation of the ΔH_f model trigonal structures of Ag_2S (space group $R\bar{3}$ and $R\bar{3}m$) shown in Fig. 1*c* are almost the same

Table 2. Predicted model cubic, tetragonal and trigonal structures of Ag_2S

Symmetry	Space group	Atom	Position and multiplicity	Atomic coordinates in model structures		
				$x / a \equiv x / a$	$y / b \equiv y / b$	$z / c \equiv z / c$
Cubic	[1] $224-Pn\bar{3}m$	Ag	$4(b)$	0.2500001	0.2500001	0.2500001
		S	$2(a)$	0	0	0
	[2] $227-Fd\bar{3}m$	Ag	$32(e)$	0.0800106	0.0800106	0.0800106
		S1	$8(a)$	0	0	0
		S2	$8(b)$	0.5	0.5	0.5
Tetragonal	[3] $116-P\bar{4}c2$	Ag1	$4(e)$	0.2303562	0.2303562	0.25
		Ag2	$4(f)$	0.2303562	0.2303562	0.75
		S1	$2(b)$	0.5	0.5	0.25
		S2	$2(c)$	0	0	0
	[4] $123-P4/mmm$	Ag1	$1(a)$	0	0	0
		Ag2	$1(b)$	0	0	0.5
		S	$1(d)$	0.5	0.5	0.5
Trigonal	[5] $148-R\bar{3}$	Ag	$2(c)$	0.2500007	0.2500007	0.2500007
		S	$1(a)$	0	0	0
	[6] $166-R\bar{3}m$	Ag1	$2(c)$	0.1249771	0.1249771	0.1249771
		Ag2	$2(c)$	0.3750229	0.3750229	0.3750229
		S1	$1(a)$	0	0	0
		S2	$1(b)$	0.5	0.5	0.5

[1] Parameters of the predicted unit cell (space group $Pn\bar{3}m$): $a = b = c = 0.544009$ nm, $Z = 2$, $V = 0.16099736$ nm^3, $\mathbf{a} = [100]_{cub}$, $\mathbf{b} = [010]_{cub}$, $\mathbf{c} = [001]_{cub}$.

[2] Parameters of the predicted unit cell (space group $Fd\bar{3}m$): $a = b = c = 1.723559$ nm, $Z = 8$, $V = 5.120101924$ nm^3, $\mathbf{a} = [100]_{cub}$, $\mathbf{b} = [010]_{cub}$, $\mathbf{c} = [001]_{cub}$.

[3] Parameters of the predicted unit cell (space group $P\bar{4}c2$): $a = b = 0.628234$ nm, $c = 0.715433$ nm, $Z = 4$, $V = 0.282365157$ nm^3, $\mathbf{a} = [100]_{tetr}$, $\mathbf{b} = [010]_{tetr}$ and $\mathbf{c} = [001]_{tetr}$.

[4] Parameters of the predicted unit cell (space group $P4/mmm$): $a = b = 0.357475$ nm, $c = 0.546104$ nm, $Z = 1$, $V = 0.069785624$ nm^3, $\mathbf{a} = [100]_{tetr}$, $\mathbf{b} = [010]_{tetr}$, $\mathbf{c} = [001]_{tetr}$.

[5] Parameters of the predicted unit cell (space group $R\bar{3}$): $a = b = c = 0.440645$ nm, $\alpha = 60.005°$, $V = 0.060506592$ nm^3, $Z = 1$.

[6] Parameters of the predicted unit cell (space group $R\bar{3}m$): $a = b = c = 0.763092$ nm, $\alpha = 33.5637°$, $V = 0.120980424$nm^3, $Z = 2$.

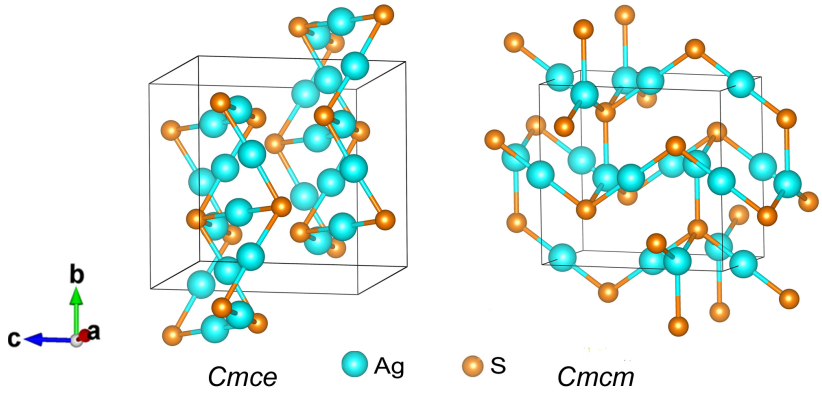

Fig. 2. Elementary cells of model orthorhombic phases of Ag_2S with space groups 64—C*mce* and 63—*Cmcm*

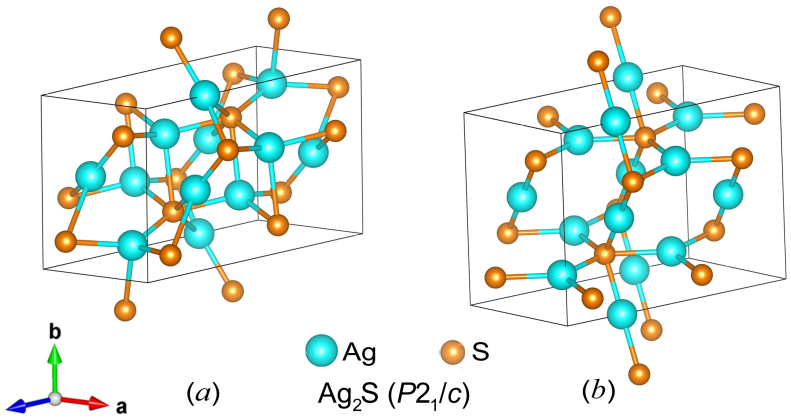

Fig. 3. Elementary cells of monoclinic (space group $P2_1/c$) phases with acanthite structure α-Ag_2S. *a* is the structure before relaxation [23], *b* is the structure after relaxation

and equal to +0.042 and + 0.041 eV/form. units, respectively (see Table 1). It is clear that the formation of these model trigonal structures of Ag_2S is also energetically unprofitable.

Thus, among cubic, tetragonal and trigonal model phases, only the predicted cubic (space group $Pn\bar{3}m$) the structure Ag_2S with the enthalpy of formation of −0.191 eV/form. units can be an alternative to the low-temperature phase of silver sulfide.

The elementary cells of the model orthorhombic phases Ag_2S with space groups *Cmc* and *Cmcm* are shown in Fig. 2.

The translation vectors and atomic coordinates in the elementary cells of orthorhombic phases are Ag_2S shown in Table 3.

The calculated enthalpy of formation of ΔH_f of these structures are equal to −0.219 and −0.199 eV/form. units, respectively (see Table. 1), therefore their formation is quite possible.

Using the USPEX code, monoclinic (space group $P2_1/c$) models of the structure α-Ag_2S (acanthite) before and after relaxation were also calculated (Fig. 3). The nonrelaxed structure corresponds to a monoclinic one (space group $P2_1/c$) the structure of acanthite α-Ag_2S is described in [23]. The initial relaxation was carried out by energy, then the structure was recalculated with more precise convergence criteria. The translation vectors and atomic coordinates in the elementary cells of unrelaxed and relaxed monoclinic (space group $P2_1/c$) phases of silver sulfide with acanthite structure of α-Ag_2S are shown in Table 4.

The enthalpy of formation of ΔH_f this monoclinic (space group $P2_1/c$) phase is Ag_2S equal to −0.219 eV/form. units (see Table. 1), i.e., the 0.02 enthalpy of relaxed acanthite is less by eV/form. units.

The relaxed monoclinic (space group $P2_1/c$) model of acanthite turned out to be the best in terms

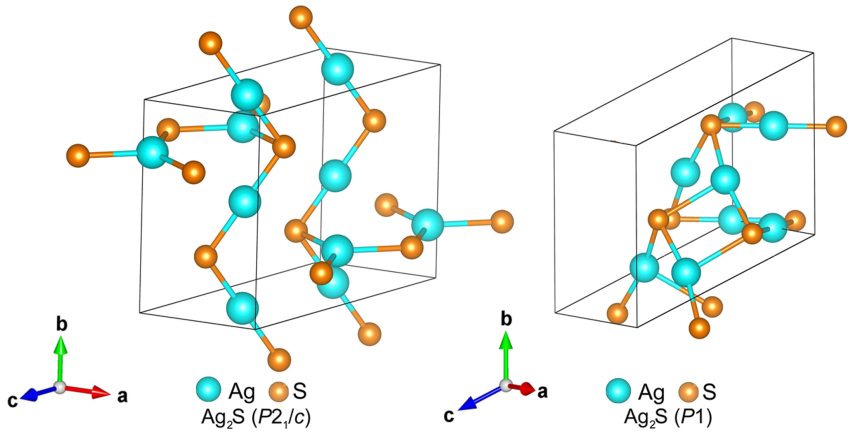

Fig. 4. The unit cell of the model monoclinic (space group $P2_1/c$) phase of Ag_2S (on the left) with the lowest enthalpy of $\Delta H_f = -0.219$ eV/form. units among the predicted monoclinic structures and the unit cell of the model triclinic (space group $P1$) phase of Ag_2S (on the right) with the lowest enthalpy of $\Delta H_f = -0.223$ eV/form. units.

Table 3. Predicted model orthorhombic structures of Ag_2S

Space group	Atom	Position and multiplicity	Atomic coordinates in model structures		
			$x / a \equiv x / a_{orthorh}$	$y / b \equiv y / b_{orthorh}$	$z / c \equiv z / c_{orthorh}$
[1] $63 - Cmcm$	Ag	$4(b)$	0	0.5	0
	Ag	$4(c)$	0	0.04657	0.25
	S	$4(c)$	0	0.68496	0.25
[2] $64 - Cmce$	Ag1	$8(e)$	0.25	0.22162	0.25
	Ag2	$8(f)$	0	0.02841	0.75496
	S	$8(f)$	0	0.72452	0.39559

[1] Parameters of the predicted unit cell (space group *Cmcm*): $a = 0.461442$ nm, $b = 0.738306$ nm, $c = 0.791054$ nm, $V = 0.269500$ nm3, $Z = 4$.
[2] Parameters of the predicted unit cell (space group *Cmce*): $a = 0.832398$ nm, $b = 0.834841$ nm, $c = 0.862424$ nm, $V = 0.599315$ nm3, $Z = 8$.

of enthalpy of formation of α-Ag_2S. The enthalpy of formation ΔH_f of an unrelaxed acanthite structure is equal to -0.033 eV/form. units, whereas the enthalpy of formation of ΔH_f of a relaxed acanthite structure is significantly less and amounts to -0.199 eV/form units (see Table 1), that's why their formation is quite possible.

The calculation showed that the X-ray image of unrelaxed acanthite coincides with experimental X-ray images of large-crystalline monoclinic (space group $P2_1/c$) acanthite α-Ag_2S with great accuracy [23]. After acanthite relaxation, the parameters of the unit cell and, accordingly, the coordinates of the Ag atoms and S were changed (see Table 4). As a result of atomic displacements in the relaxed phase, a more ordered arrangement of atoms, especially atoms Ag, is observed compared with unrelaxed acanthite (see Fig. 3).

In particular, atoms Ag are predominantly located in atomic planes perpendicular to the axes *a* and the *c* unit cell. Note that in numerous experimental studies of silver sulfide, summarized in [5], only unrelaxed acanthite was observed as a low-temperature phase, regardless of the method and conditions of synthesis.

The calculation of other model structures of Ag_2S shown that the monoclinic structure of acanthite described in the literature [4, 23] α-Ag_2S is not the only possible and most energetically advantageous low-temperature phase of silver sulfide. As a result

Table 4. Monoclinic (space group 14 – $P2_1/c$) α-Ag_2S structures of acanthite before relaxation [27] and after relaxation

Monoclinic (space group $P2_1/c$) α-Ag_2S	Atom	Position and multiplicity	Atomic coordinates in model structures		
			$x / a \equiv x / a_{mon}$	$y / b \equiv y / b_{mon}$	$z / c \equiv z / c_{mon}$
1) Unrelaxed unit cell [27]	Ag1	$4(e)$	0.07157	0.48487	0.80943
	Ag2	$4(e)$	0.27353	0.67586	0.56247
	S	$4(e)$	0.4922	0.2341	0.13217
2) Relaxed unit cell	Ag1	$4(e)$	0.04498	0.74996	0.47750
	Ag2	$4(e)$	0.50004	0.00001	0.25002
	S1	$4(e)$	0.31581	0.25002	0.34210

[1)] Parameters of an unrelaxed unit cell (space group $P2_1/c$): a = 0.42264 nm, b = 0.69282 nm, c = 0.953171 nm, α = 90°, β = 125.554°, γ = 90°, V = 0.227068 nm^3, Z = 4.
[2)] Parameters of a relaxed unit cell (space group $P2_1/c$): a = 0.435628 nm, b = 0.791975 nm, c = 0.871257 nm, α = 9°, β = 116.111°, γ = 90°, V = 0.269911 nm^3, Z = 4.

of calculations, it was possible to find a monoclinic (space group $P2_1/c$) phase Ag_2S (Fig. 4, left) with a lower energy in the ground state compared with relaxed acanthite.

The translation vectors and atomic coordinates in the unit cell of this monoclinic (spatial group $P2_1/c$) phase of silver sulfide are shown in Table 5.

As a result of the modeling of other possible structures of Ag_2S, it was possible to establish that the monoclinic phases of silver sulfide Ag_2S are not the most energetically advantageous low-temperature phases. Calculations allowed us to find the triclinic (space group $P1$) phase Ag_2S (Fig. 4, right). This phase Ag_2S has the lowest cohesion energy of $E_{coh} = -8.304$ eV/form. units and enthalpy of formation of $\Delta H_f = -0.223$eV/form. units (see Table. 1) in the ground state at $T = 0$ K and $P = 0$. The translation vectors and atomic coordinates in the unit cell of the triclinic (space group $P1$) phase of Ag_2S are shown in Table 5.

Calculations of model structures of silver sulfide Ag_2S using the USPEX evolutionary algorithm [10 –13] have shown that a decrease in phase symmetry Ag_2S from cubic, tetragonal and trigonal to orthorhombic, monoclinic and, especially, triclinic crystallographic systems is accompanied by a decrease in their energy and the formation of the most energetically advantageous structures. Indeed, the transformation of a high-temperature cubic (space group $Im\bar{3}m$) arginite β-Ag_2S into any model structure of Ag_2S will occur with a decrease in symmetry.

Crystallographic point groups and all the elements of their symmetry are listed in the monograph [24] in accordance with the notation adopted in [25]: the 48 elements of the complete cubic symmetry group $m\bar{3}m$ (O_h) are sequentially designated from h_1 to h_{48}.

The point group $m\bar{3}m$ (O_h) of the BCC-argentite β-Ag_2S includes all the 48 symmetry elements of the $h_1 h_{48}$ cubic group [24], i.e., $N_{h-arg} = 48$. The rotational decrease in symmetry N_{rot} is equal to the ratio of the number of symmetry elements of the argentite point group to the number of symmetry elements $N_{h-phase}$ included in the point group of the considered model structure Ag_2S, i.e., $N_{rot} = N_{h-arg} / N_{h-phase} = 48 / N_{h-phase}$. The decrease in translational symmetry is equal to the relative change in the volume of the unit cell when the argentite is transformed into a model structure of Ag_2S. The total decrease in symmetry $N_{tot} = N_{rot} \times N_{tr}$ is the product of a rotational decrease in symmetry

Table 5. Predicted model monoclinic (space group $14-P2_1/c$) and triclinic (space group $1-P1$) structures of Ag_2S

Symmetry and space group	Atom	Position and multiplicity	Atomic coordinates in model structures		
			$x / a \equiv x / a$	$y / b \equiv y / b$	$z / c \equiv z / c$
[1] Monoclinic (space group $14 - P2_1/c$)	Ag1	$4(e)$	0.52641	0.24248	0.47333
	Ag2	$4(e)$	0.02658	0.25188	0.47346
	S	$4(e)$	0.52441	0.39461	0.22983
[2] Triclinic (space group $1-P1$)	Ag1	$1(a)$	0.86160	0.11768	0.65392
	Ag2	$1(a)$	0.18251	0.45397	0.34767
	Ag3	$1(a)$	0.68702	0.45957	0.35685
	Ag4	$1(a)$	0.02431	0.56922	0.00840
	Ag5	$1(a)$	0.52371	0.56411	0.00802
	Ag6	$1(a)$	0.36410	0.10713	0.66484
	Ag7	$1(a)$	0.00327	0.00177	0.00153
	Ag8	$1(a)$	0.50720	0.00312	0.01042
	S1	$1(a)$	0.62789	0.41309	0.70515
	S2	$1(a)$	0.90766	0.15612	0.30911
	S3	$1(a)$	0.11466	0.85369	0.70273
	S4	$1(a)$	0.42086	0.71554	0.31158

[1] Parameters of an unrelaxed monoclinic unit cell (space group $P2_1/c$):
$a = 0.590253$ nm, $b = 0.863974$ nm, $c = 0.836796$ nm, $\alpha = 90^\circ$, $\beta = 135.1413^\circ$, $\gamma = 90^\circ$, $V = 0.301002437$ nm^3, $Z = 4$.
[2] Parameters of a triclinic unit cell (space group P1): $a = 0.593602$ nm, $b = 0.706832$ nm,
$c = 0.781798$ nm, $\alpha = 116.4408^\circ$, $\beta = 110.9258^\circ$, $\gamma = 91.3246^\circ$, $V = 0.267753731$ nm^3, $Z = 4$.

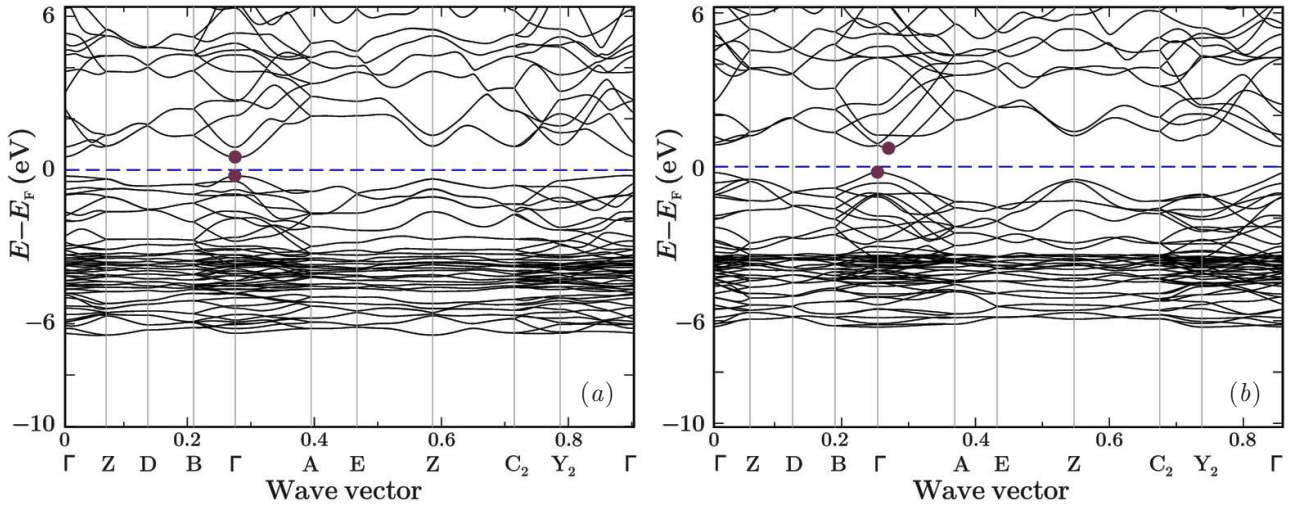

Fig. 5. Zonal structure of unrelaxed (*a*) and relaxed (*b*) monoclinic (space group $P2_1/c$) acanthite α-Ag_2S

by a decrease in translational symmetry. For example, during the transition of argentite to monoclinic acanthite, the α-Ag_2S volume of the unit cell is doubled, i.e., $N_{tr} = 2$; the point group $2/m(C_{2h})$ of acanthite includes $N_{h-acanth} = 4$elements of symmetry h_1, h_4, h_{25} and h_{28}, therefore $N_{rot} = 12$, and the total decrease in symmetry N_{tot} is 24. The decrease in the symmetry of the N_{tot} predicted model phases of Ag_2S relative to the arginite is shown in Table 1. Using the example of silver sulfide structures with the same monoclinic (space group $P2_1/c$) symmetry, it is especially clearly seen that the greatest decrease in symmetry leads to the formation of phases with the lowest enthalpy of formation (see Table 1).

All the considered model low-temperature phases of Ag_2S are very similar in their electronic structure. In their band structure, a band gap of 0.6 up to 1.5 eV is observed, indicating the semiconductor properties of the predicted phases of Ag_2S. For relaxed structures, the Ag_2S band gap width $E_g$varies from 1.02up to 1.16 eV and is close to the experimentally measured values of 0.9–1.1 eV [5].

The zonal structure of unrelaxed and relaxed monoclinic (space group$P2_1/c$) acanthite α is α-Ag_2S shown in Fig. 5*a* and 5*b*, respectively.

It is clearly seen that unrelaxed acanthite is a straight-band semiconductor. As a result of relaxation, the band structure has changed somewhat, since an electron located near the bottom of the conduction band has acquired a pulse that differs from the pulse of an electron located near the maximum of the valence band. Thus, the relaxed acanthite becomes an indirect semiconductor.

The densities of the states of unrelaxed and relaxed monoclinic (spatial group $P2_1/c$) acanthite Ag_2S are shown in Fig. 6*a* and 6*b*, respectively.

The structure of unrelaxed acanthite, formed according to X-ray diffraction data [23], has a significantly smaller band gap, 0.72 eV, compared with $E_g = 1.02$ eV of relaxed acanthite α-Ag_2S. The states near the Fermi level are formed by 4*d*-orbitals Ag, the states are 3*p*S most pronounced in the energy ranges below 0.5– 2.0 and 4.5– 6.0 eV relative to the Fermi level.

Total and partial densities of the predicted triclinic states (space group *P*1) the structures of Ag_2S with the lowest enthalpy of formation of $\Delta H_f =$ $= -0.223$ eV/form. units (see Table 1) are shown in Fig. 6*c*. The band gap of E_g triclinic silver sulfide is 1.16 eV. The band gap of $E_g$orthorhombic (space group *Cmce*) silver sulfide is 1.04 eV (Fig. 6*d*), which is slightly larger than $E_g$relaxed acanthite. For monoclinic (space group$P2_1/c$) acanthite and orthorhombic (space group *Cmce*) silver sulfide, the edge of the valence band near the Fermi level has a slope (see Fig. 6*a*, 6*b* and 6*d*) and resembles experimental optical spectra [26, 27]. The width of the acanthite valence band is approximately 4–6 eV, which coincides with the data of the experiment on photoelectron spectroscopy of silver sulfide [8, 28].

Predicted cubic (space group $Pn\bar{3}m$) The structure of Ag_2S was proposed as a derivative of the structure of the BCC (space group $Im\bar{3}m$) of the argentite β-Ag_2S. The enthalpy of formation of $\Delta H_f = -0.191$ eV/form. units of this structure is one

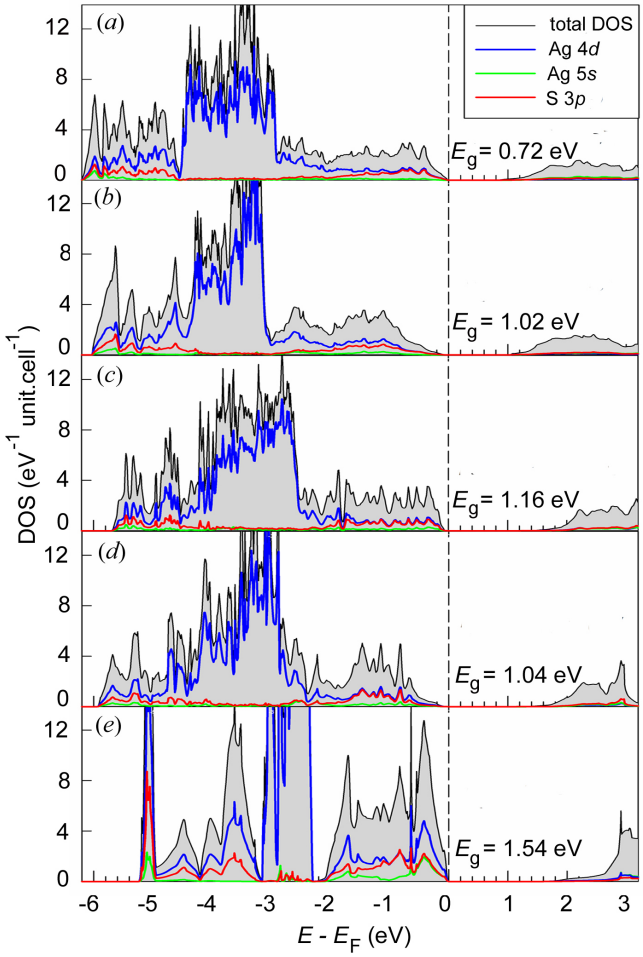

Fig. 6. Total and partial Ag4*d*-, Ag5*s*- and S3*p*-densities of states of model structures of silver sulfide. Unrelaxed (*a*) and relaxed (*b*) monoclinic (space group $P2_1/c$) acanthite α-Ag_2S; *c* — predicted triclinic (space group $P1$) Ag_2S structure, *d* — predicted orthorhombic (space group *Cmce*) Ag_2S structure, *e* — relaxed cubic (space group $Pn\bar{3}m$) Ag_2 structure.

of the smallest among the predicted phases of silver sulfide. The electronic structure of the predicted cubic (space group $Im\bar{3}m$) phase Ag_2S (see Fig. 6*e*) differs markedly from the densities of states of other low-temperature phases Ag_2S. The valence band of a cubic (space group $Pn\bar{3}m$) The Ag_2S structure is split, and the band gap is 1.54 eV, i.e., about 50% larger than $E_g$other predicted structures of Ag_2S.

We will find channels of structural disorder–order phase transitions associated with the formation of the predicted monoclinic (space group $P2_1/c$) unrelaxed acanthite α-Ag_2S and cubic (space group $Pn\bar{3}m$) phases of $Ag_2S$from BCC-argentite (space group $Im\bar{3}m$) of β-Ag_2S. According to [4], the translation vectors of an elementary cell of an ideal monoclinic (space group $P2_1/c$) phase α-Ag_2S in a basic lattice with a BCC structure have the form

$$\mathbf{a}_{P2_1/c} = \left(\mathbf{a}_{bcc} + \mathbf{b}_{bcc} - \mathbf{c}_{bcc}\right)/2 = \\ = \left\{1/2 \quad 1/2 \quad -1/2\right\}_{bcc},$$

$$\mathbf{b}_{P2_1/c} = \left(\mathbf{a}_{bcc} - \mathbf{b}_{bcc}\right) = \left\{1 \quad -1 \quad 0\right\}_{bcc}$$

and

$$\mathbf{c}_{P2_1/c} = 2\mathbf{c}_{bcc} = \left\{0 \quad 0 \quad 2\right\}_{bcc}.$$

The basis vectors of the $\mathbf{b}_i^*$inverse lattice,

$$\mathbf{b}_1^* = \mathbf{a}_{P2_1/c}^*, \quad \mathbf{b}_2^* = \mathbf{b}_{P2_1/c}^*, \quad \mathbf{b}_3^* = \mathbf{c}_{P2_1/c}^*,$$

they are determined through translational vectors $\mathbf{a}_i$ ($\mathbf{a}_1 \equiv \mathbf{a}_{P2_1/c}^*, \mathbf{a}_2 \equiv \mathbf{b}_{P2_1/c}^*, \mathbf{a}_3 \equiv \mathbf{c}_{P2_1/c}^*$) of elementary cell according to the formula

$$\mathbf{b}_t^* = 2\pi \frac{\mathbf{a}_j \times \mathbf{a}_k}{\mathbf{a}_1 \cdot (\mathbf{a}_2 \times \mathbf{a}_3)}, \qquad (2)$$

where $i, j, k = 1,2,3$.

According to the calculation, the vectors of the inverse lattice of unrelaxed monoclinic acanthite α are α-Ag_2S equal

$$\mathbf{a}^* = \left\{1 \quad 1 \quad 0\right\}, \mathbf{b}^* = \left\{-1/2 \quad -1/2 \quad 0\right\},$$

$$\mathbf{c}^* = \{1/4 \quad 1/4 \quad 1/2\}$$

in units $2\pi/a$. The first Brillouin zone of the basic volume-centered cubic lattice has the shape of a rhombododecahedron. The combination and translation of the found vectors of the inverse lattice showed that in the first Brillouin zone of the basic volume-centered cubic nonmetallic sublattice of argentite there are six nonequivalent superstructural vectors. Two of them are superstructural wave vectors

$$\mathbf{k}_9^{(1)} = \mathbf{b}_3/2, \quad \mathbf{k}_9^{(2)} = \left(\mathbf{b}_2 - \mathbf{b}_1\right)/2,$$

which belongs to a six — ray Lifshitz star $\left\{\mathbf{k}_9\right\}$with elements representing symmetry h_1, h_2, h_5, h_6, h_9 and h_{11}. The four other superstructural vectors are superstructural wave vectors

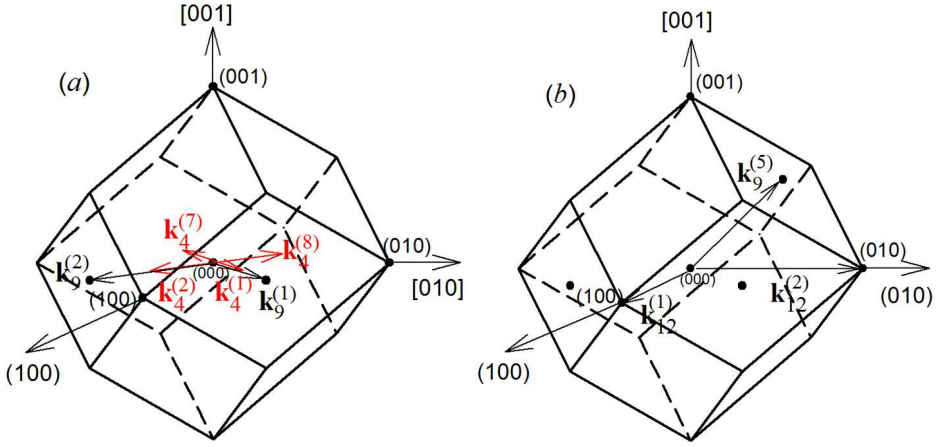

Fig. 7. Superstructural vectors of the inverse lattice of unrelaxed monoclinic (space group $P2/c$) acanthite α-Ag_2S (*a*) and predicted cubic (space group $Pn\bar{3}m$) phases Ag_2S (*b*) included in the corresponding channels of disorder–order phase transitions, and their position in the first Brillouin zone of the BCC lattice of disordered argentite β-Ag_2S

$$\mathbf{k}_4^{(1)} = \mu\mathbf{b}_3 = \left(1/4 \quad 1/4 \quad 0\right),$$

$$\mathbf{k}_4^{(2)} = \mu\left(\mathbf{b}_2 - \mathbf{b}_1\right) = \left(1/4 \quad -1/4 \quad 0\right)$$

and opposite wave vectors

$$k_4^{(7)} = -\mathbf{k}_4^{(1)}, \quad k_4^{(8)} = -\mathbf{k}_4^{(2)}.$$

These vectors are rays of a 12 ray-bearing non-Lifshitz star $\{\mathbf{k}_4\}$with the current parameter $\mu_4 = 1/4$ and symmetry elements h_1, h_2, h_5, h_6, h_9, h_{11}, h_{25}, h_{26}, h_{29}, h_{30}, h_{33} and h_{35}. Here and further, the numbering and description of the stars of the $\{\mathbf{k}_s\}$ wave vectors of the inverse lattice of the BCC structure and their rays are given in accordance with [29],

$$\mathbf{b}_1 = \left(0 \quad 1 \quad 1\right), \quad \mathbf{b}_2 = \left(1 \quad 0 \quad 1\right), \quad \mathbf{b}_3 = \left(1 \quad 1 \quad 0\right)$$

— the structural vectors of the inverse lattice of the basic BCC lattice in units $2\pi/a$; the rotational symmetry elements of the h_i cubic group in matrix form are described in [24]. These six superstructural vectors enter the phase transition channel associated with the formation of the monoclinic (space group $P2_1/c$) α-Ag_2S superstructure under discussion (Fig. 7*a*).

The translation vectors of a primitive cubic (space group $Pn\bar{3}m$) phase cell Ag_2S in a basic lattice with a BCC structure have the form

$$\mathbf{a}_{Pn-3m} = \left(1/2 \quad 1 \quad 0\right), \quad \mathbf{b}_{Pn-3m} = \left(-1/2 \quad 1 \quad 0\right),$$

$$\mathbf{c}_{Pn-3m} = \left(1/2 \quad 0 \quad 1\right).$$

According to the calculation according to formula (2), the basis vectors of the $\mathbf{b}_i^*$inverse lattice of the cubic phase Ag_2S,

$$\mathbf{b}_1^* = \mathbf{a}_{Pn-3m}, \quad \mathbf{b}_2^* = \mathbf{b}_{Pn-3m}, \quad \mathbf{b}_3^* = \mathbf{c}_{Pn-3m},$$

found through the translational vectors of a primitive cubic cell, are equal to

$$\mathbf{a}^* = \left\{1 \quad 1/2 \quad -1/2\right\}, \quad \mathbf{b}^* = \left\{1 \quad -1/2 \quad -1/2\right\},$$

$$\mathbf{c}^* = \left\{0 \quad 0 \quad 1\right\}$$

in units $2\pi/a$. Combining and translating these vectors, we obtain that in the first Brillouin zone of the basic body-centered cubic nonmetallic sublattice there are three nonequivalent superstructural vectors:

$$\mathbf{k}_{12}^{(1)} = \mathbf{c}^* = \left(0 \quad 0 \quad 1\right), \quad \mathbf{k}_{12}^{(2)} = \mathbf{a}^* - \mathbf{b}^* = \left(0 \quad 1 \quad 0\right),$$

$$\mathbf{k}_{12}^{(5)} = -\mathbf{b}^* + \mathbf{k}_{12}^{(3)} = \left(0 \quad 1/2 \quad 1/2\right).$$

Two superstructural vectors belong to a 3 radial Lifshitz star $\mathbf{k}_{12}$ with elements representing symmetry h_1, h_5 and h_9 and one vector belongs to a 6 radial Lifshitz star $\mathbf{k}_9$ with elements representing symmetry h_1, h_2, h_5, h_6, h_9 and h_{11}. These three superstructural vectors enter the phase transition channel associated with the formation of a cubic (space group $Pn\bar{3}m$) superstructure Ag_2S (Fig. 7*b*).

Thus, it was possible to find channels of disorder–order transitions associated with the formation of the

predicted monoclinic (space group $P2_1/c$) unrelaxed acanthite α-Ag_2S and cubic (space group $Pn\bar{3}m$) phases of Ag_2S from the volume-centered (spatial group $Im\bar{3}m$) argentite β-Ag_2S.

The elastic stiffness constants of the c_{ij} predicted model phases of silver sulfide were Ag_2S calculated in the VASP software package. The elastic compliance constants were s_{ij} determined by calculating the matrices (**S**) of the elastic compliance constants, which are the inverse of the matrices (**C**), i.e., $(\mathbf{S}) = (\mathbf{C})^{-1}$. We found the matrices (**S**) of the predicted structures by Ag_2S calculating the inverse matrices using the program [30] for calculating the inverse matrices.

The calculated elastic constants were c_{ij} used to evaluate the mechanical stability of the predicted model phases of Ag_2S using the Born criteria [31] and the necessary and sufficient conditions for the elastic stability of various crystal systems described in [21].

A necessary but not sufficient condition for the mechanical stability of a crystal of any symmetry is the positivity of all diagonal elements of the matrix of elastic stiffness constants, i.e., $c_{ii} > 0$, $i = 1-6$.

The stability criteria of cubic crystals have the form [21, 31]

$$c_{ii} > 0, \quad c_{11} > c_{12}, \quad c_{44} > 0, \quad c_{11} + 2c_{12} > 0.$$

These criteria are fulfilled for cubic (space group $Fd\bar{3}m$ and $Pn\bar{3}m$) model phases of Ag_2S, therefore they are mechanically stable. However, the positive enthalpy of the formation of a cubic phase with a space group $Fd\bar{3}m$ excludes the existence of such a phae.

The conditions of mechanical stability of tetragonal and trigonal crystals have the form [21]

$$c_{11} > c_{12}, \quad c_{44} > 0, \quad c_{66} > 0,$$
$$(c_{11} + c_{12})c_{33} > 2c_{13}^2$$

and

$$c_{11} > c_{12}, \quad c_{44} > 0, \quad (c_{11} + c_{12})c_{33} > 2c_{13}^2,$$
$$(c_{11} - c_{12})c_{44} > 2c_{14}^2 + 2c_{15}^2.$$

The elastic stiffness constants of the considered model tetragonal (space group $P4/$and $P\bar{4}c2$) and trigonal (space group $R\bar{3}$ and $R\bar{3}m$) phases do of Ag_2S not satisfy these conditions, therefore the predicted tetragonal and trigonal phases are Ag_2S mechanically unstable.

The necessary and sufficient conditions of mechanical stability [21] are fulfilled for orthorhombic (space groups *Cmcm* and *Cmce*) model phases of Ag_2S, therefore these phases are mechanically stable. For nonrelaxed and relaxed monoclinic (space group $P2_1/c$) acanthite α-Ag_2S constants of elastic stiffness

$$c_{ii} > 0, \quad c_{22} + c_{33} > 2c_{23},$$
$$c_{11} + c_{22} + c_{33} > 2(c_{12} + c_{13} + c_{23}), \quad c_{33}c_{55} > c_{35}^2$$

and

$$c_{44}c_{66} > c_{46}^2$$

they satisfy the necessary and sufficient conditions of mechanical stability, therefore, these monoclinic (space group $P2_1/c$) phases of Ag_2S are mechanically stable. For the triclinic (space group $P1$) model phase of the Ag_2S elastic stiffness constant $c_{ii} > 0$. With this in mind, it can be assumed that the triclinic (space group $P1$) model phase Ag_2S satisfies the conditions of mechanical stability and is mechanically stable.

Thus, among the considered low-temperature model phases of silver sulfide, only cubic (space group $Pn\bar{3}m$), orthorhombic (space group *Cmcm* and *Cmce*)monoclinic (spatial group $P2_1/c$) and triclinic (space group $P1$) structures of Ag_2S have mechanical stability.

Calculated elastic stiffness constants of the predicted cubic (space group $Pn\bar{3}m$) the structures are Ag_2S are

$$c_{11} = 46.2, \quad c_{12} = 43.2, \quad c_{44} = 1.2 \text{ Pa}.$$

Cubic crystals have anisotropy of elastic properties [32]. According to [32], the dependences of the elastic modulus on the crystallographic direction can be represented through the trigonometric functions of the guide angles θ. Another way of representing the dependences of the Young's modulusE_{hkl}, Poisson's constant, μ_{hkl} and the shear modulus of G_{hkl} cubic crystals from the crystallographic direction $[hkl]$ is implemented in [33]. The presence of angular dependences of the elastic modulus or dependences

of the modules on the crystallographic direction $[hkl]$ indicates anisotropy of the elastic properties of cubic crystals.

The elastic matrix of cubic crystals includes only three independent positive constants of elastic stiffness c_{11}, c_{12} and c_{44}. According to [33], the elastic modulus of Young E and shear G and the Poisson constant of μ cubic crystals have the form

$$E_{hkl} = \frac{(c_{11}-c_{12})(c_{11}+2c_{12})c_{44}}{(c_{11}+c_{12})c_{44}-(2c_{44}-c_{11}+c_{12})(c_{11}+2c_{12})\Gamma}, \quad (3)$$

$$G_{hkl} = \frac{2(c_{11}-c_{12})c_{44}}{4c_{44}-6(2c_{44}-c_{11}+c_{12})\Gamma}, \quad (4)$$

$$\mu_{hkl} = \frac{1}{2} - \frac{E_{hkl}}{2(c_{11}+2c_{12})}. \quad (5)$$

In formulas (3)–(5), the value Γ is the anisotropy factor of cubic crystals,

$$\Gamma = \frac{h^2k^2+h^2l^2+k^2l^2}{\left(h^2+k^2+l^2\right)^2}.$$

The modulus of all-round compression of B cubic crystals does not depend on the direction $[hkl]$ [32] and is equal to

$$B = \frac{c_{11}+2c_{12}}{3}. \quad (6)$$

The calculated elastic stiffness constants of high–temperature silver sulfide – body-centered cubic (space group $Im\bar{3}m$) argentite β-Ag_2S at $T = 470$ K are equal to

$$c_{11} = 89.6, \quad c_{12} = 4.0, \quad c_{44} = 17.2 \text{ GPa}.$$

As already noted, argentite β-Ag_2S is a high-temperature phase of silver sulfide, with respect to which the predicted low-temperature structures Ag_2S are ordered phases. The calculated space

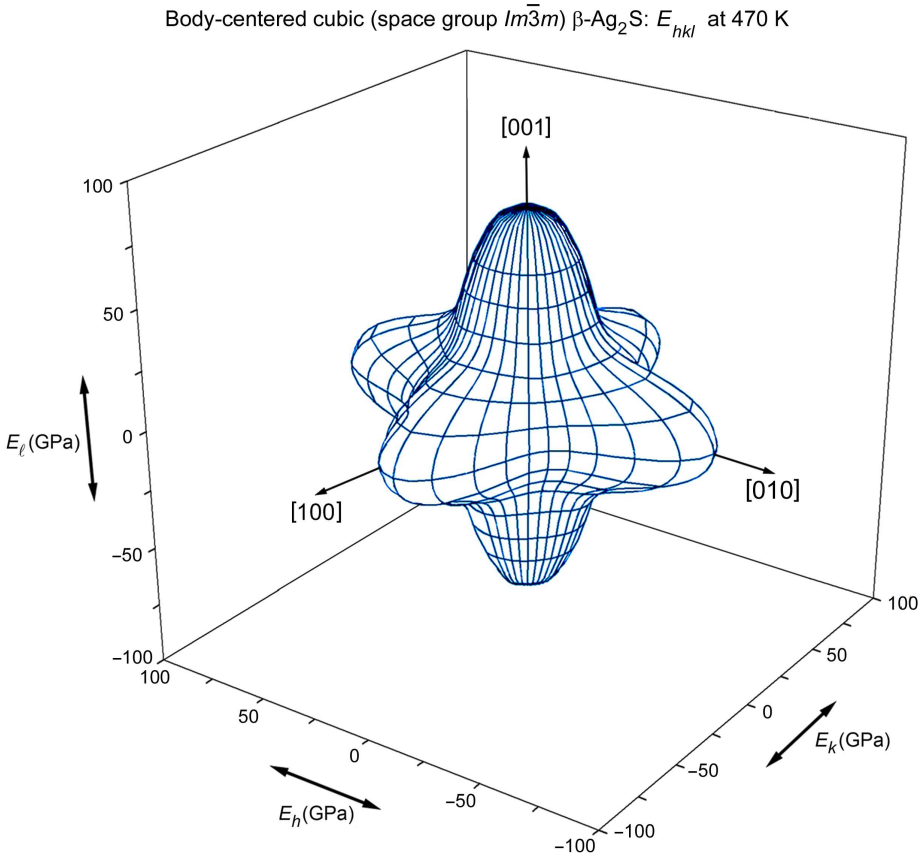

Fig. 8. Spatial distribution of the elastic modulus E_{hkl} of a body-centered cubic (space group $Im\bar{3}m$) argentite β-Ag_2S at temperature 470 K

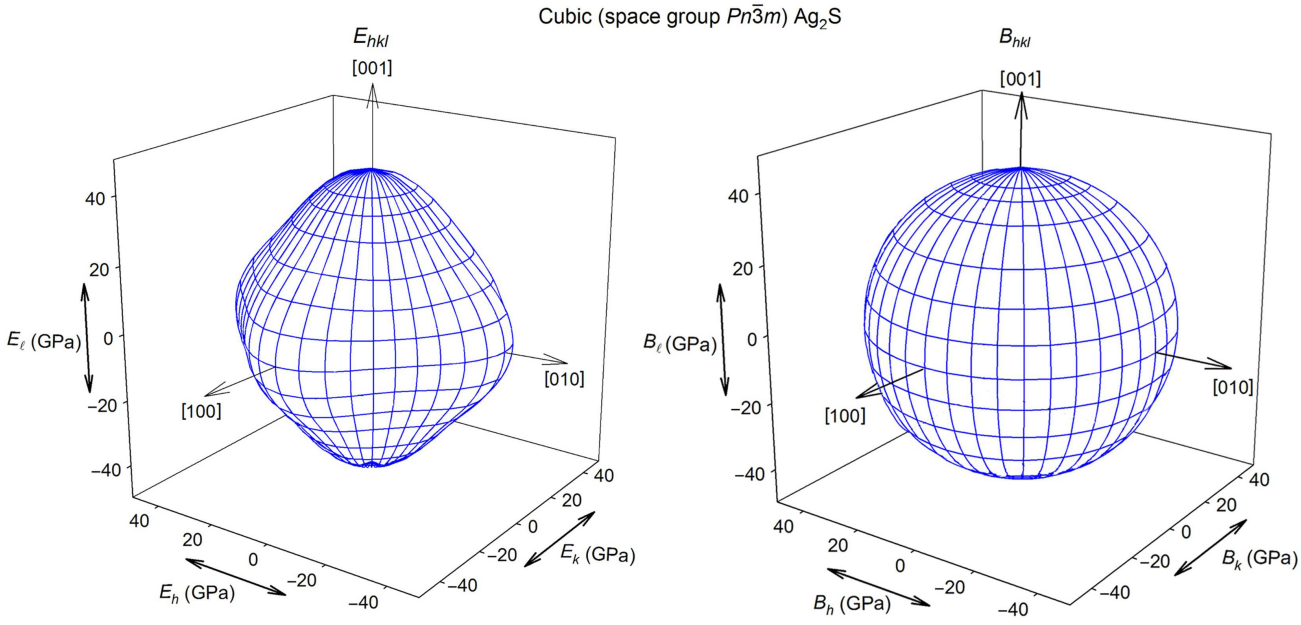

Fig. 9. Spatial distributions of the Young's modulus E_{hkl} (*a*) and the all-round compression modulus B (*b*) of the predicted cubic (space group $Pn\bar{3}m$) silver sulfide Ag_2S

three-dimensional distribution of the elastic modulus of E_{hkl} BCC-argentite β-Ag_2S at temperature 470 K is shown in Fig. 8.

The maximum value of the elastic modulus of E_{hkl} argentite β-Ag_2S at $T = 470$ K in the directions $[100]$, $[010]$, $[001]$ and in the opposite directions is equal to 83.3 GPa, the minimum value of 40.14 GPa is the elastic modulus of E_{hkl} argentite β-Ag_2S has in the directions $[\pm 0.7071 \pm 0.7071 \pm 0.7071]$.

The spatial three-dimensional distributions of the Young's E_{hkl} modulus and the all-round compression modulus of B_{hkl} cubic (space group $Pn\bar{3}m$) silver sulfide Ag_2S are shown in Fig. 9. The largest Young's modulus $E_{max} = 44.5$ GPa is observed for external deformation applied along one of the crystallographic directions $[001]$, $[010]$ or $[100]$. The lowest value of the $E_{min} = 35.7$ GPa is observed in eight equivalent directions $[\pm 1 \pm 1 \pm 1]$ at points with coordinates $h = k = l = \pm 0.7071$. The all-round compression modulus is the B_{hkl} same in all directions $[hkl]$ and has a spherical shape, the calculated modulus of B_{hkl} cubic (space group $Pn\bar{3}m$) silver sulfide Ag_2S is 44.2 GPa.

The Zener anisotropy criterion is used to evaluate the anisotropy of cubic crystals [34]

$$A_{an} = \frac{2c_{44}}{c_{11} - c_{12}}.$$

The Zener criterion $A_{an} = 1$ corresponds to perfectly isotropic cubic crystals. For argentite β-Ag_2S Zener criterion $A_{an} = 0.4$, which indicates a significant anisotropy of the elastic properties of argentite. For the discussed cubic (space group $Pn\bar{3}m$) silver sulfide Ag_2S the criterion $A_{an} = 0.8$ indicates a slight anisotropy of the elastic properties of the predicted cubic (space group $Pn\bar{3}m$) silver sulfide, especially in comparison with argentite.

4. CONCLUSION

The USPEX evolutionary algorithm was used to search for model low-temperature phases of silver sulfide. The possibility of the formation of Ag_2S phases having cubic, tetragonal, orthorhombic, trigonal, monoclinic and triclinic symmetries is considered. The calculation of the enthalpy of formation showed that the formation of low-symmetric phases is most favorable energetically Ag_2S. The mechanical stability of all Ag_2S predicted phases has been determined. It is shown that the cubic (space group $Pn\bar{3}m$), orthorhombic (space groups $Cmcm$ and $Cmce$) and monoclinic (space groups $P2_1$ and $P2_1/c$) predicted phases of Ag_2S are mechanically stable. It is established that in the band structure of all the considered low-temperature model phases of silver sulfide there is a band gap indicating their semiconductor properties. Channels of disorder–order transitions

associated with the formation of low-temperature unrelaxed monoclinic (space group $P2_1/c$) acanthite α-Ag_2S and cubic (space group $Pn\bar{3}m$) silver sulfide Ag_2S from disordered argentite have been found. The spatial distributions of the Young's E_{hkl} modulus and the all-round compression modulus B_{hkl} of cubic (space group $Pn\bar{3}m$) silver sulfide Ag_2S are determined, and a weak anisotropy of the elastic properties of the predicted cubic silver sulfide is established.

FUNDING

The study was carried out with the support of the Russian Science Foundation (project 19-79-10101-П) at the Institute of Solid State Chemistry of the Ural Branch of the Russian Academy of Sciences. The calculations were performed on the Uran supercomputer at the Institute of Mathematics and Mechanics of the Ural Branch of the Russian Academy of Sciences.

REFERENCES

1. R. C. Sharma and Y. A. Chang, Bull. Alloy Phase Diagrams **7**, 263-269 (1986).

2. W. T. Thompson and S. N. Flengas, Can. J. Chem. **49**, 1550-1563 (1971).

3. S. I. Sadovnikov, A. I. Gusev, and A. A. Rempel, Phys. Chem. Chem. Phys. **17**, 12466-12471 (2015).

4. R. Sadanaga and S. Sueno, Mineralog. J. Japan. **5**, 124-148 (1967).

5. S. I. Sadovnikov and A. I. Gusev, J. Mater. Chem. A **5**, 17676-17704 (2017).

6. S. I. Sadovnikov, A. I. Gusev, and A. A. Rempel, Phys. Chem. Chem. Phys. **17**, 20495-20501 (2015).

7. O. Alekperov, Z. Jahangirli and R. Paucar, Phys. stat. sol.(b) **253**, 1-7 (2016).

8. S. Kashida, N. Watanabe, T. Hasegawa, H. Iida, M. Mori, and S. Savrasov, Sol. State Ionics **158**, 167-175 (2003).

9. S. F. Etris, In *Kirk-Othmer Encyclopedia of Chemical Technology*, *Metals and Alloys*, Wiley, New York (2001), vol. 4, pp.761-803.

10. Universal Structure Predictor: Evolutionary Xtallography. Manual. Version 9.4.4 (http://uspex-team.org)

11. A. R. Oganov and C. W. Glass, J. Chem. Phys. **124**, paper 244704 (2006).

12. A. R. Oganov, A. O. Lyakhov, and M. Valle, Accounts Chem. Res. **44**, 227-237 (2011).

13. A.O. Lyakhov, A. R. Oganov, H. T. Stokes, Q. Zhu, Comp. Phys. Comm. **184**, 1172-1182 (2013).

14. W. Kohn and L. J. Sham, Phys. Rev. **140**, A1133-A1138 (1965).

15. J. P. Perdew, K. Burke, and M. Ernzerhof, Phys. Rev. Lett. **77**, 3865-3868 (1996).

16. G. Kresse and D. Joubert, Phys. Rev. B **59**, 1758-1775 (1999).

17. G. Kresse and J. Furthmüller, Comput. Mater. Sci. **6**, 15-50 (1996).

18. Vienna Ab-initio Simulation Package. VASP the GUIDE. April 20, 2016 (http://cms.mpi.univie.ac.at/VASP/)

19. P. E. Blöchl, O. Jepsen, and O. K. Andersen, Phys. Rev. B **49**, 16223-16233 (1994).

20. Y. Hinuma, G. Pizzi, Y. Kumagai, F. Oba, and I. Tanaka, Comp. Mater. Sci. **128**, 140-184 (2017).

21. F. Mouhat and F-X. Coudert, Phys. Rev. B **90**, paper 224104 (2014).

22. K. Momma and F. Izumi, J. Appl. Crystallogr. **44**, 1272-1276 (2011).

23. S. I. Sadovnikov, A. I. Gusev, and A. A. Rempel, Superlat. Microstr. **83**, 35-47 (2015).

24. A. I. Gusev, A. A. Rempel, and A. J. Magerl, *Disorder and Order in Strongly Nonstoichiometric Compounds. Transition Metal Carbides*, *Nitrides and Oxides*, Springer-Verlag, Berlin – Heidelberg - New York (2001). 608 pp.

25. O. V. Kovalev, *Irreducible Representations of the Space Groups*, Gordon & Breach, New York (1965). 210 pp.

26. A. I. Kryukov, O. L. Stroyuk, N. N. Zin'chuk, A. V. Korzhak, and S. Ya. Kuchmii, J. Mol. Catal. A **221**, 209-221 (2004).

27. S. I. Sadovnikov, Yu. V.Kuznetsova, and A. A. Rempel, Nanostr. Nano-Object. **7**, 81-91 (2016).

28. Q. Liu, Y. Pu, Zh. Zhao, J. Wang, and D. Wang, Transact. Tianjin Univ. **26**, 273-282 (2020).

29. O. V. Kovalev, *Representations of the Crystallographic Space Groups*: *Irreducible Representations*, *Induced Representations and Corepresentation*, Gordon & Breach Science Publ., Yverdon - Paris – Berlin - London – Tokyo – Amsterdam (1993). 2nd ed. 390 pp. https://matrix.reshish.ru

31. M. Born, Math. Proc. Camb. Phil. Soc. **36**, 160-172 (1940).

32. R. E. Newnham, *Properties of Materials. Anisotropy*, *Symmetry*, *Structure*, Oxford Univ. Press, New York (2005). P.109-113.

33. T. Gnäupel-Herold, P. C. Brand, and H.J. Prask, J. Appl. Crystallogr. **31**, 929-935 (1998).

34. C. Zener, *Elasticity and Anelasticity of Metals*, University of Chicago, Chicago (1948). 170 pp.